ASME Journal of Turbomachinery
Online journal at:
https://asmedigitalcollection.asme.org/turbomachinery

Tassilo von Mueller[1]
Department of Engineering Science,
University of Oxford,
Oxford OX1 3PJ, UK
e-mail: tassilo.vonmueller@eng.ox.ac.uk

David Bacci
Department of Engineering Science,
University of Oxford,
Oxford OX1 3PJ, UK
e-mail: david.bacci@eng.ox.ac.uk

Augustin Wambersie
Department of Engineering Science,
University of Oxford,
Oxford OX1 3PJ, UK
e-mail: augustin.wambersie@eng.ox.ac.uk

Tsun Holt Wong
Department of Engineering Science,
University of Oxford,
Oxford OX1 3PJ, UK
e-mail: holt.wong@eng.ox.ac.uk

Peter Ireland
Department of Engineering Science,
University of Oxford,
Oxford OX1 3PJ, UK
e-mail: peter.ireland@eng.ox.ac.uk

Dougal Jackson
Rolls-Royce plc,
Derby DE24 8BJ, UK
e-mail: Dougal.Jackson@Rolls-Royce.com

Effect of Blockages on Film Effectiveness on the Pressure Surface of a Turbine Blade

An experimental and numerical study was conducted on fan-shaped holes on the pressure surface of a high-pressure turbine blade. Blockages in these film holes can arise through dirt accumulation as well as erosion of the thermal barrier coatings. The objective was to study the effects of partial blockages on film cooling effectiveness. Similar studies have been conducted on flat surfaces. This study includes the effect of curvature, which has been shown to be influential on film cooling performance. A blade with a single row of nominal fan-shaped holes at a lateral inclination of 30 deg was tested and used as the baseline performance. Blockage cases were then tested at various blowing ratios, with partial blockages in the throat as well as partial lidding in the fan exit of the film hole. The experiments were carried out using pressure-sensitive paint (PSP) in the high-velocity 2D linear cascade experimental facility at the Oxford Thermofluids Institute, using engine-representative Mach and Reynolds numbers. The results show that lidding with up to 0.5 blocking ratio (defined as the ratio of lidded length to the length of the film hole exit, in the film hole plane) only has a minor impact on film effectiveness, while lidding with 0.75 blocking ratio as well as throat blockage both result in significant deterioration of film cooling effectiveness. The effect of blockages on the discharge coefficient was also studied, and only blockages in the throat were found to reduce the discharge coefficient.
[DOI: 10.1115/1.4067688]

Keywords: film cooling, pressure-sensitive paint, film hole blockage, heat transfer and film cooling

1 Introduction

Modern gas turbine manufacturers are continually attempting to increase the thermal efficiency of gas turbines. This process has caused turbine entry temperatures to exceed the material properties of most turbine components. To prevent a breakdown of parts, film cooling is widely used in order to reduce metal temperature and thereby increase the longevity of turbine blades. Coolant air is taken from the compressor and bled through film holes to create a layer of cold air between the hot combustion gases and the airfoil surface. Another technology used to shield the turbine blades is the use of thermal barrier coatings (TBCs). However, TBCs can sometimes alter the dimensions of the film hole, leading to a change in performance of the film hole. Film holes are generally manufactured by laser drilling or electrode discharge machining (EDM). However, these processes can sometimes create irregular film holes. EDM can result in molten metal splatter settling in the film hole. Additionally, ingested particles from the atmosphere often deposit on the blades and inside film holes, causing erosion and modification of film holes. The study by Dunn [1] shows the damaging effect of ingestion of volcanic ash on high-pressure turbine blades. Some of these particles are of very small orders of magnitude and therefore impossible to be captured by air filtration. It is therefore crucial for turbine blade manufacturers to understand the issue that is caused by the alteration of film hole designs and ultimately its effect on film cooling effectiveness.

The current study aims to add to the understanding of blockage effects on film cooling performance. Film effectiveness measurements of design intent and defective fan-shaped film holes were taken at matched pressure ratios (PRs), simulating the environment that defective film holes would experience in an engine. Measurements were taken using pressure-sensitive-paint (PSP).

[1]Corresponding author.

Contributed by the International Gas Turbine Institute (IGTI) of ASME for publication in the Journal of Turbomachinery. Manuscript received August 13, 2024; final manuscript received October 5, 2024; published online February 18, 2025. Tech. Editor: David G. Bogard.

2 Relevant Past Studies

2.1 Effect of Blockages on Film Effectiveness. Most studies in laboratory conditions involve design-intent film holes which ensure repeatability and ease of comparison. Schroeder and Thole [2] performed a study on the performance of the widely studied "7-7-7" baseline fan-shaped film cooling hole on a flat plate test facility. Its performance was characterized by varying density ratios (DRs), blowing ratios (BRs), and turbulent intensities. The results were then compared against multiple other geometries with varying hole dimensions available in the literature. However, few studies have examined the performance of defective film holes and their detrimental effect on film cooling effectiveness. Bunker [3] performed one of the first studies on partially blocked cylindrical and fan-shaped holes due to TBC coatings on a flat plate test section. For a fan-shaped hole, the blockage was applied so that it only affected the diffuser part of the hole without creating any blockage in the throat. Only centerline adiabatic effectiveness was measured, and it was found that the blockage created a reduction of 20–30% effectiveness in the near-hole region. Past $x/D = 40$, there was no significant difference between the pristine and the partially blocked hole. Whitfield et al. [4] studied the effect of TBC blockages on film cooling effectiveness in cylindrical and fan-shaped holes on a flat plate test facility. Blockages decreased the area ratio, thereby reducing the mass flowrate through the film holes at the same PR. For matched BR, blocked holes produced narrower film coverage and lower centerline film effectiveness. At higher BR, effectiveness for blocked holes was up to 60% worse than the baseline. A study by Jovanović et al. [5] looked at the presence of imperfections in cylindrical film holes and compared their effect on film cooling effectiveness to a benchmark hole. This was conducted in a flat plate test facility. A half-torus was used as the imperfection and placed at various locations in the film hole. The results show varying effects with the imperfection in the middle of the throat having a little effect on film effectiveness at low velocity ratios. In contrast, the imperfection placed at the hole exit improved film effectiveness under the same conditions.

Numerical studies were also performed on blocked film holes. Wang et al. [6] investigated blockage effects on cylindrical film holes using Reynolds-averaged Navier–Stokes (RANS) computational fluid dynamics (CFD) simulation. Blockages were found to lead to more penetration of the coolant into the mainstream and stronger counterrotating vortex pair. Coolant coverage and cooling effectiveness were significantly reduced. Zhang et al. [7] performed a similar study on blocked cylindrical and fan-shaped holes with blockages in different locations of the film hole exit. A blockage in the form of an annulus, similar to the one in the study by Jovanović et al. [5] led to a decrease in film effectiveness by up to 80%. On the other hand, blockages at the leading and trailing edges of the film hole exit led to slight increases in film effectiveness. Thermal fields showed that the blockages changed the velocity field and in some cases led to better coolant attachment downstream of the film hole.

The study by Whitfield et al. [4] is most similar to the current study in that it studies blockages in fan-shaped holes with results presented in the same way as in the current study (Bunker [3] only studied centerline effectiveness). Therefore, a comparison between the current study and that of Whitfield et al. [4] is of the most relevance. However, the two main differences between Whitfield et al. [4] and the current study is the addition of a lateral inclination angle as well the presence of the curvature of the pressure surface in the current study. Given these two effects, a comparison will have its limitations, and ideally, a study with the same geometry on a pressure surface would be taken as a benchmark. However, given the lack of such a study, the impact of lateral inclination and the effect of the curvature need to be understood before making a comparison with the study by Whitfield et al. [4].

2.2 Effect of Curvature on Film Effectiveness. Most studies on film cooling holes have been conducted on flat plates because they represent a simpler flow and therefore allow understanding of the performance of jets on a fundamental level. However, real engines require film cooling on curved surfaces that vary in performance to flat plates, which miss the effects of pressure gradient and curvature. Heat transfer coefficients and turbulent properties are greatly impacted by curvature. Schwarz et al. [8] showed that flows over concave surfaces—such as that of a pressure surface—are generally characterized by worse film effectiveness. Flows over a concave surface are accelerated toward the center of curvature and therefore drawn away from the high-pressure concave wall. Bacci et al. [9] conducted a study comparing the performance of a row of fan-shaped holes on flat plate to vane pressure and suction surface. The direct comparison between flat plate and pressure surface shows a significantly worse performance for the pressure surface at a blowing ratio of 1. At a blowing ratio of 2, the difference is slightly reduced. The study by Zhang et al. [10] found a similar result, when comparing the performance of fan-shaped holes on a concave and flat plate test section, although the difference was not quite as pronounced. Indeed, it was found that over the range of blowing ratios between 0.5 and 2, the flat plate consistently showed an increase of 0.02–0.03 η in area-averaged film effectiveness over the concave test case.

2.3 Effect of Lateral Inclination in Fan-Shaped Holes on Film Effectiveness. Most studies of film cooling holes and, in particular defective film cooling holes, were done without any lateral inclination. However, modern gas turbine blades use film holes with lateral inclination, which have shown to increase coverage and ensure better protection of the blade. Since this study involves a lateral inclination angle of 30 deg, it is important to understand the effect this might have on film cooling effectiveness. Lateral inclination has been studied for much longer on cylindrical holes than on fan-shaped holes. The general understanding is that lateral inclination for cylindrical film holes improves lateral spreading and reduces coolant penetration into the mainstream, improving film effectiveness overall [11]. Lateral inclination angles in fan-shaped holes have been investigated much less. Gritsch et al. [12] studied the effect of 45 deg and 90 deg lateral inclination in fan-shaped holes (among other geometric factors). It was found that the lateral injection angle only had a weak impact on film effectiveness at low to medium blowing ratios. At higher blowing ratios, the straight hole was slightly better. Heneka et al. [13] tested laidback fan-shaped holes with varying lateral hole angles (among other geometric variations). The authors found that lateral inclination of 30 deg slightly enhanced film effectiveness at both lower and higher blowing ratios. However, the enhancement was only seen near the film hole exit, and no effect of lateral inclination was seen far downstream of the hole exit. It was hypothesized that the lateral inclination increased the interaction between coolant and mainstream, thereby reducing the coolant capacity of the film. Dittmar et al. [14] performed a study comparing a row of fan-shaped holes with and without a 35 deg lateral injection angle. Similar to the study by Heneka et al. [13], it was found that the lateral injection angle slightly increased film cooling effectiveness and only in the near-hole region. This was the case for both low and high blowing ratios. Overall, the literature suggests that lateral inclination has almost no effect or only a very slight increase in film effectiveness for fan-shaped holes. The studies by Gritsch et al. [12], Heneka et al. [13], and Dittmar et al. [14] were all made using diffuser-shaped holes with forward expansion. The current study was equally done with forwardly expanded fan-shaped holes.

3 Experimental Approach

3.1 High-Velocity 2D Linear Cascade. The experiments presented in this study were conducted in the high-velocity 2D cascade at the University of Oxford. The test section is a single-blade passage that follows the midspan streamlines of an engine-representative high-pressure turbine blade. Perspex walls were

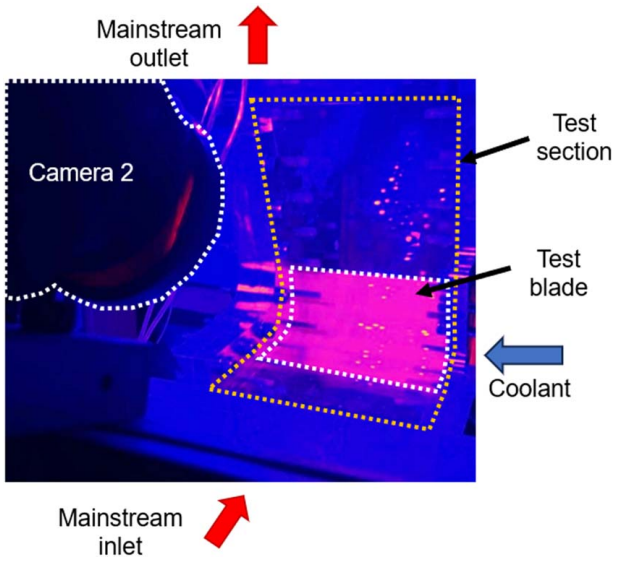

Fig. 1 View of test section under UV lighting

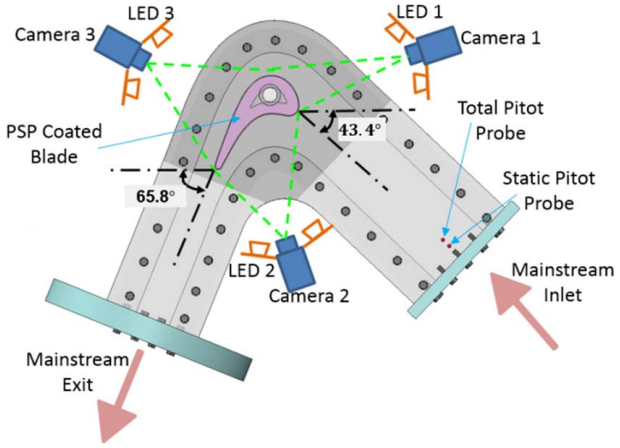

Fig. 2 Schematic of the test facility [15]

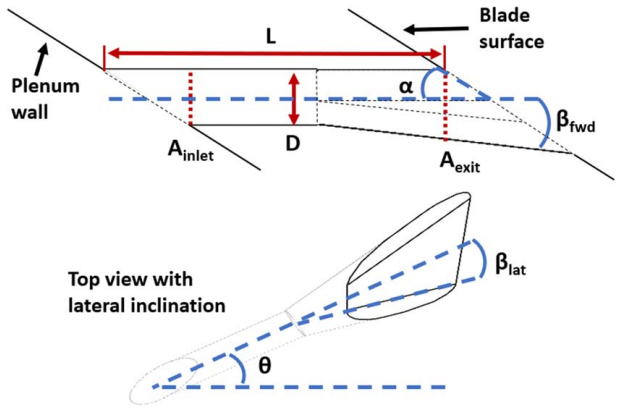

Fig. 3 Definition of the baseline geometry

designed to simulate adjacent rotor blades' midpitch streamlines, while also allowing for full visual access of the blade. Figure 1 shows a view of the pressure surface of a test blade under UV lighting. The view is taken from the perspective of "camera 2" as shown in the schematic in Fig. 2 from the work by Ngetich et al. [15] (note that the picture taken in Fig. 1 is slightly out of line with camera 2, explaining the angled orientation of the mainstream air to the blade). The pink dots in Fig. 1 on the perspex walls are reflections on the perspex from the UV LED lights. The blue reflections stem from the UV lighting located above camera 2 (marked "camera 2" in Fig. 1). The operating conditions of the test facility as well as data capture, experimental procedure, and instrumentation are also described in more detail in the work by Ngetich et al. [15]. Additionally, inlet turbulence intensity was measured at 11% with a hot wire located a chord length upstream of the leading edge of the blade. The integral length scale was found to be $\Lambda_x/D = 6$, which roughly corresponds to the size of the flow-straightener hex mesh located upstream of the test section. Test pieces were coated with a white primer to increase the signal, followed by UniFib PSP. The mechanism and measurement technique of PSP is well documented in the work by Han and Rallabandi [16]. A total pressure probe in the plenum of the test blades was used to measure the PR across the film holes, defined as the total coolant pressure over the local mainstream external static pressure ($\frac{p_{c,0}}{p_{\infty,s}}$). Test blades were tested for the following PR: 1.06, 1.09, 1.12, 1.17, 1.22, 1.27, 1.35, and 1.40. This was representative of a range of blowing ratios between 0.5 and 1.6, depending on the geometry.

3.2 Test Matrix and Design Assessment. Test blades were built from acrylic resin with a 3D Systems Multijet MJP 2500 Plus in-house printer. This provides a nearly adiabatic surface (thermal conductivity of $= 0.12\,\mathrm{W/m \cdot K}$). Pin gauging of film holes was used to confirm the diameter measurement. With an initial test piece, shrinkage of 5–10% was identified with the film hole diameters after the part was cured. A correction factor was then applied to the design in order to manufacture film holes with the intended diameter. All the parts were printed from hub (coolant inlet side) to tip.

The baseline film hole is shown in Fig. 3: the top part shows geometric features, while the bottom part shows the internal geometry of the film hole in a top view. Note how the lateral inclination changes the appearance of the film hole in comparison to the study by Schroeder and Thole [2]. For clarity, future geometry figures will not be shown in the lateral inclination view and without plenum and blade surface walls. The geometry is a laidback fan-shaped hole with a cylindrical portion followed by a diffused outlet in the forward and lateral direction. Geometric features are given in Table 1. A_{exit} was measured at the breakout point with the surface. Representative defective geometries presented later in this study all share the same baseline geometry design. All defects characterize different ways in which particles have been observed to deposit in the film holes of engine-run turbine blades, thereby modifying the intended geometry.

Two of the defects examined in this study were designed with internal blockages in their cylindrical portion. The "0.75D throat" case had a throat with a diameter reduced by 25%. This was designed by revolving an arc (radius of curvature of $R/D = 8.2$ and length of $l/D = 2.9$ around the axis of the film hole, creating a gradual reduction in diameter by a maximum of 25% at the throat (see Fig. 4 for a cross-sectional view of the 0.75D geometry). The second geometry was designed with a hemisphere of diameter 0.4D placed at the exit of the cylindrical section of the fan-shaped hole (see Fig. 5 for a cross-sectional view of the "0.4D globule" geometry). An initial concern was that this defect would be so small that it would not be discernible among the roughness of the

Table 1 Geometric dimensions of baseline geometry

Features	L/D	β_{fwd}	β_{lat}	α	θ	AR	P/D
	6.5	6.4	12.5	27.3	30	1.95	4.8

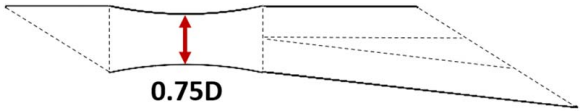

Fig. 4 Cross section of a blocked hole with 0.75D throat

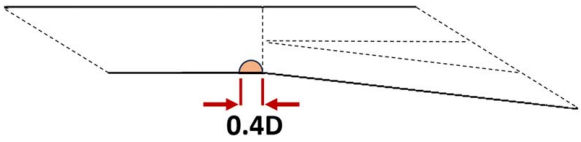

Fig. 5 Cross section of a blocked hole with 0.4D globule

part. Using an Alicona Infinite Focus optical microscope, a scan of a high-resolution replication material pushed into the film hole was taken and shown in Fig. 6. The globule was measured to have a diameter of 0.43D, confirming that the 3D printing was able to resolve this defect.

The "fan exit deposition" geometry represents molten metal splatter in the fan exit, which builds up during the EDM process. Hemispheres measuring 0.6D in diameter were placed in the fan exit. Figure 7 shows a CAD image of the fan exit with the hemispheres as well as two scans of the film hole exit using an optical microscope (the left scan is of a replication material, while the right one represents a scan of the part). This scan confirmed once again the ability to resolve a deposition size of 0.63D compared to 0.6D design intent.

In some cases, deposits progressively build up in the fan exit to the point where they eventually block the film hole exit completely. This refers to lidding, and the defects here represent partial lidding (though they are referred to as "lidding" here). Figure 8 shows a lidded geometry, modeled to be flush with the blade surface. The ratio of lidding was defined as the ratio of lidded length (t) over the total length (C) from trailing to leading edge of the film hole

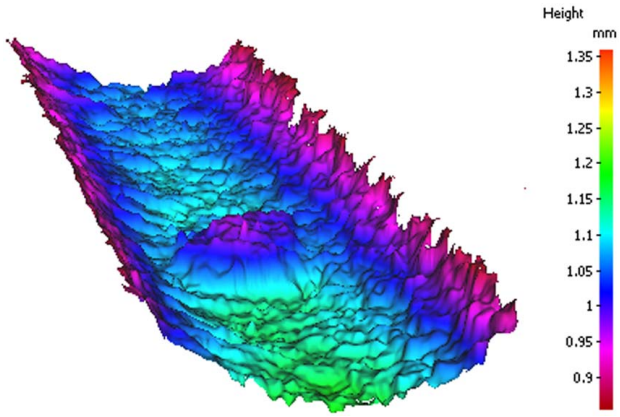

Fig. 6 View of the 0.4D globule with an optical microscope

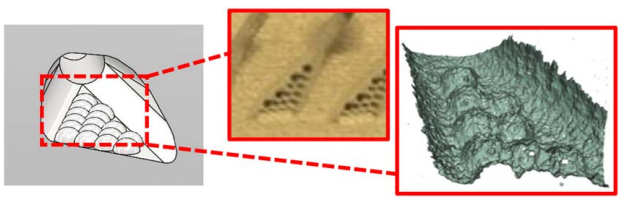

Fig. 7 Fan exit deposition

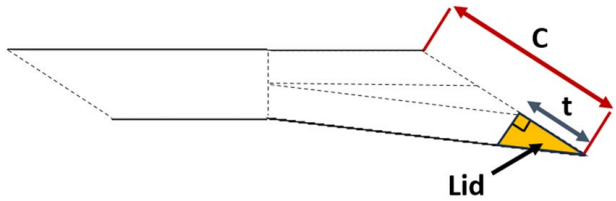

Fig. 8 Lid definition as a ratio of t/C

exit. Ratios t/C of 25%, 50%, and 75% were tested which correspond to fan exit areas at the blade surface of respectively 65%, 55%, and 22% of the baseline (note that these are not the same as the exit area defined in Fig. 3). The lid edge was designed to be perpendicular to the blade surface to model the most aggressive buildup of particles seen in engine-run parts. An inspection of the 3D print revealed a fillet at the edge ($R/D = 0.23$). The defect is built parallel to the downstream edge of the film hole, and therefore, it is not symmetric. Figure 9 shows a close-up view of the lidded film holes including a view of the blade geometry. The location of the film holes on the turbine blade can also be seen—in this study, they are located in the late pressure surface.

Table 2 presents an overview of the various geometries tested and the groupings on each blade. Four different test blades were designed with a total of 15 film holes, all fed from the same plenum. Of the four test blades, three were designed with three different geometries and with five film holes each. A baseline geometry was put on each of the three blades and always at the hub of the blade (toward the coolant feed side). The geometries located at the tip and midspan were all defective fan-shaped geometries. Three justifications were studied to confirm that a comparison of film holes in the span was possible. First, based on the theory of exhaust manifolds presented in the work by Miller [17], uniform flow distribution would be achieved across the blade span with a branch loss ratio of less than 0.5. In fact, the branch loss ratio was found to be 0.04, well below the limit described by Miller. Second, a baseline test case was run with a full row of design-intent fan-shaped holes (shown in Sec. 5). The spanwise-averaged film effectiveness showed little variation between tipwards, midspan, and hubwards-located film holes. Third, CFD analysis showed little variation in mass flowrate across the 15 film holes (at most a difference of 2%).

The arithmetic mean roughness (Ra) of parts was measured in order to understand how the measurement instrumentation (i.e., the PSP coat) would affect the surface topology. Since the interior of film holes was inaccessible to the microscope, multiple roughness measurements were taken upstream and downstream of the film holes. A mean roughness of $\mathrm{Ra}/D = 0.010$ was found for printed parts, compared to $\mathrm{Ra}/D = 0.0057$ for parts coated with

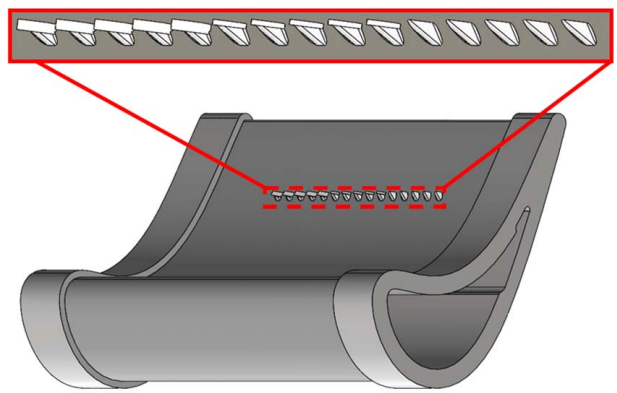

Fig. 9 View of blade geometry including a close-up view of 50%, 25%, and baseline film holes

Table 2 Geometric dimensions of defects tested

Test blade	Film hole	t/C	AR	Defect size
Baseline	Baseline	–	1.95	–
Blade 1	0.75D throat	–	3.50	0.25D
	0.4D globule	–	2.07	0.4D
Blade 2	25% lid	0.25	1.95	–
	50% lid	0.5	1.95	–
Blade 3	75% lid	0.75	1.95	–
	Fan exit deposition	–	1.95	0.6D

paint. These measurements indicated that the coating of PSP smoothens the surface and almost halves the Ra value.

3.3 Measurement Uncertainty. The two main sources in the PSP measurement are the uncertainty in the measured camera intensity as well as the temperature uncertainty. Han and Rallabandi [16] showed that PSP is highly sensitive to changes in temperature, and temperature effects could be minimized if reference and test images were taken at the same temperature. However, this proved to be quite difficult, and even minor changes in temperature between test and reference cases can cause significant uncertainty in η. An estimation of the uncertainty due to temperature was made by using the perturbation method as described in the work by Moffat [18]. A perturbation of the temperature term was done across multiple datasets spanning the entire film effectiveness range and averaging the uncertainty at each effectiveness value (to the nearest 0.01 η). The PSP uncertainty due to the intensity for the test facility was quantified in the work by Wambersie [19]. In general, precision uncertainty for the intensity term can be minimized by taking multiple images and averaging the intensities. In the current study, 50 images were taken for each case and averaged. Absolute values of film effectiveness uncertainty are given in Table 3. The uncertainty at low effectiveness is higher than at high effectiveness because the intensity scales exponentially with oxygen partial pressure. Note that the uncertainty refers to single data points and not averaged data. Additionally, the uncertainty presented here refers to single-component PSP.

In order to get an understanding of the reproducibility of the data, the baseline blade was tested five times at PR = 1.27 and over the course of several days. The results are shown in Fig. 10 including analytical uncertainty bands. It can be seen that there is a maximum variation of 0.01 in film effectiveness between the five cases was found in the exit of the film hole at $x/D = 3$ (for $\eta = 0.15$). The maximum variation increased to 0.025 at $x/D = 26$ (for $\eta = 0.15$). These values are slightly higher than the analytical uncertainty. This might be due to PSP degradation and other factors not considered in the uncertainty calculation. However, the behavior of low uncertainty at higher film effectiveness and higher uncertainty at lower film effectiveness supports the expected uncertainty distribution given in Table 3.

The uncertainty in BR can be attributed to the following measurements (all uncertainties reported represent a 95% confidence interval): pressure (±1000 Pa), temperature (±0.5 K), mass flowrate (0.8% of reading ±0.2% of flow meter scale), and diameter measurement (pin gauging was used with a precision of 0.01 mm). Using the perturbation method described by Moffat [18], an uncertainty of 0.03 was found for a nominal BR of 1.07. The uncertainties given here also apply to all other independent measurements during a test run.

Table 3 Absolute values of film effectiveness η measurement uncertainty

Nominal η	Measurement uncertainty
0.1	0.0108
0.2	0.0092
0.4	0.0060
0.6	0.0046
0.8	0.0034
0.95	0.0021

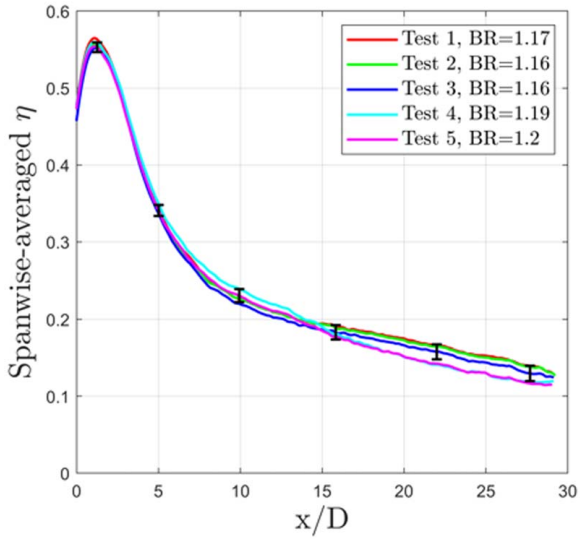

Fig. 10 Comparison of repeat testing of baseline blade at matched PR = 1.17

3.4 Flow Results and Discharge Coefficients. In the design phase, the assumption was made that the film holes fed from a plenum would all have the same mass flowrate, no matter their location across the span. However, introducing geometric variations in the form of defects might change the flow distribution, even though in most cases, the minimum flow area was the same (except for the blade with internal blockages). Therefore, flow tests were conducted through separate experiments after PSP testing, in a similar way to the flow tests described by Snyder and Thole [20]. For every flow test, two geometries were blocked off with a sealant, and the mass flowrate through the five film holes of each geometry was measured over a range of pressure ratios. A low mass flow meter was used specifically for this experiment, in order to reduce uncertainty in the mass flow measurement. Measured mass flowrates were then converted to a nondimensional flow parameter $(\dot{m}(RT_c)^{0.5}/(P_cA_c))$ to account for changes in gas pressure and temperature across tests. Ultimately, the flow parameter curves were then used to calculate the mass flowrate through each of the geometries during PSP tests, based on the pressure ratio across the film holes. Knowing the mass flowrate, BR was calculated using Eq. (1), where mean values ρ_∞ and u_∞ are measured.

$$\mathrm{BR} = \frac{\rho_c u_c}{\rho_\infty u_\infty} = \frac{\dot{m}_c/A}{\rho_\infty u_\infty} \tag{1}$$

As aforementioned, the area A was found through pin gauging. While it is acknowledged that BR of individual holes might vary, this method allows for a comparison of mean BR across geometries.

Discharge coefficients (C_D) were calculated using the methodology described by Gritsch et al. [21] for fan-shaped holes. The total pressure of the coolant was found using a total pressure measurement of the plenum of the test blades. The diameter used to calculate C_D was taken to be A_{inlet}, which was the same for all test cases. The results are shown in Fig. 11.

All the discharge coefficients were found to be between 0.6 and 0.82. Only the defect with a blockage in the throat caused a significant drop in C_D. The baseline case had one of the higher discharge

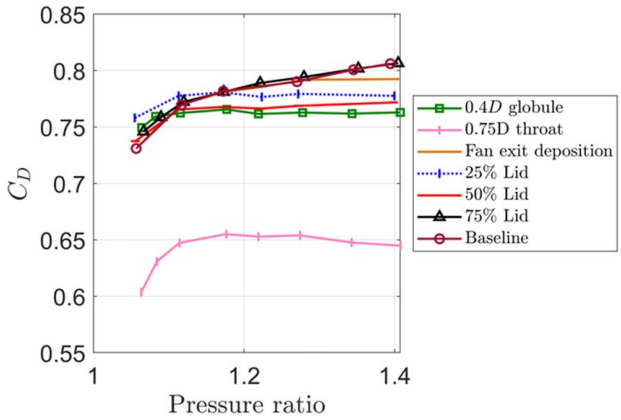

Fig. 11 Discharge coefficients for the test cases

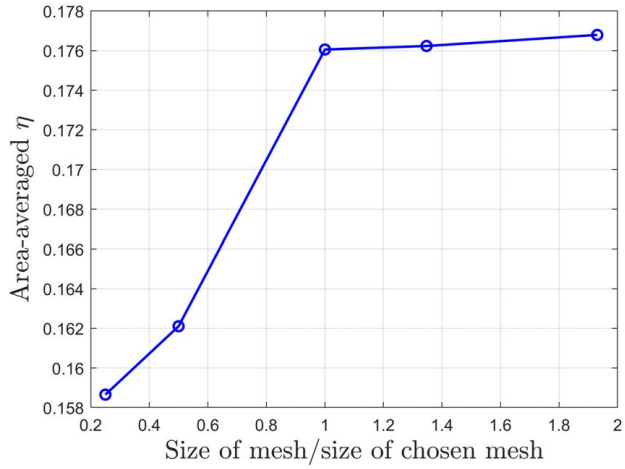

Fig. 13 Mesh independence study at BR = 0.5 for the baseline case

coefficients, which is to be expected given the larger exit expansion compared to the other cases. Interestingly, the 75% lidding and fan exit deposition case had discharge coefficients very similar to the baseline. One might expect some of the lidded holes to show a bigger drop in C_D. However, apart from the two cases with internal blockage (0.75D throat and 0.4D globule), the minimum flow area was always the throat of the film hole, and therefore, the assumption was that the mass flowrate was governed by A_{inlet}. Minor changes in C_D were attributed to film hole roughness.

4 Numerical Method

A RANS-based steady simulation was conducted using ansys fluent 2023 R1. The k-ω shear stress transport turbulence model was chosen, and the species transport model was enabled in order to model the mixing of coolant nitrogen and mainstream air. The standard law of the wall modified for roughness was implemented. This was chosen because the influence of roughness on film effectiveness was shown to be far from inconsequential [22,23]. For a smooth wall, the velocity profile in the log-law region follows Eq. (2):

$$U^+ = \frac{1}{\kappa}\log(Ey^+) \tag{2}$$

where κ and E represent empirical coefficients found by fitting the logarithmic profile to experimental data. Nikuradse [24] showed that the velocity profile for a rough wall has the same slope as that of a smooth wall, only shifted downward due to the roughness effect. For a rough wall, Eq. (2) is modified to account for the additional shear stress from the roughness elements on the surface. For that purpose a correction ΔB is applied, depending on the size and uniformity of the roughness elements. The log-law modified for roughness then becomes Eq. (3):

$$U^+ = \frac{1}{\kappa}\log(Ey^+) - \Delta B \tag{3}$$

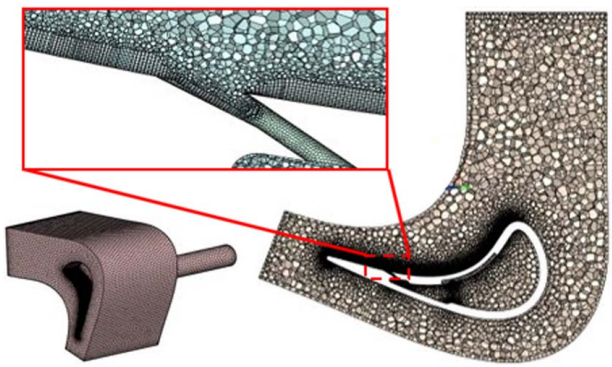

Fig. 12 View of mesh domain including close-up view of mesh refinement near the film hole

An unstructured polyhedral mesh was generated using FLUENT MESHING 2023 R1 with prism layers. The mesh modification for the RANS roughness model requires the first cell layer height to be larger than the sand grain roughness k_s. The first cell height was set to 20% larger than k_s. The average value of y^+ in the region was 36, with a minimum y^+ of 30 at any cell in order to ensure the law of the wall is used as a wall function. The only roughness parameter available in this study was the Ra measured using an optical microscope. Previous studies by Adams et al. [25] and Young [26] have found a good fit for a conversion factor of $k_s = 6\text{Ra}$. This conversion factor was employed in the current study. Figure 12 shows the mesh of the domain including a view of the mesh refinement at the pressure surface and in the film holes in a slice view of the mesh domain. In order to generate the domain, the test blade was extracted from the fluid domain, leaving the solid parts of the blade empty. The domain includes part of the coolant pipe, which feeds into the plenum of the test blade. To ensure a fine enough mesh, a mesh independence study was performed by comparing area-averaged film effectiveness for BR = 0.5. A mesh size of approximately 7.2 million cells was chosen with little variation shown in area-averaged film effectiveness results for larger mesh sizes. The results are shown in Fig. 13, representing the number of cells in each case divided by 7.2 million cells chosen for this study.

Walls were treated as adiabatic, no slip walls. All mainstream, coolant inlet and exit pressure and temperature conditions were obtained from measurements during the experiments discussed in this study. Inlet turbulence was set to 11% with an integral length scale of $\boldsymbol{\Lambda_x/D = 6}$ as measured with a hot wire. Mainstream gas was set to air while coolant was set to nitrogen in order to model the mass transfer analogy in PSP experiments more closely. Adiabatic film effectiveness was therefore quantified as the nitrogen species concentration. A pressure-based solver was used for CFD calculations. Additionally, a second-order flow discretization scheme was applied to all variables. Convergence of the solution was considered when root-mean-squared (RMS) residuals had decreased by at least two orders of magnitude. Mass flow imbalance at this point was recorded at 0.0013%. Jones et al. [27] conducted a study on the usefulness of RANS calculations for the prediction of film cooling. They found that while velocity and thermal fields matched quite well inside and at the exit of the holes, RANS failed to accurately model the mixing between the coolant and

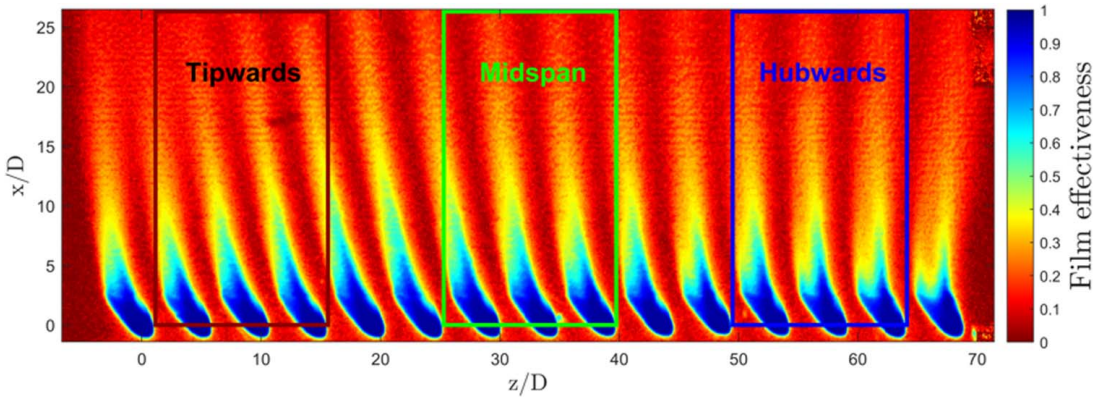

Fig. 14 Adiabatic film effectiveness contour for the baseline geometry BR = 1.2

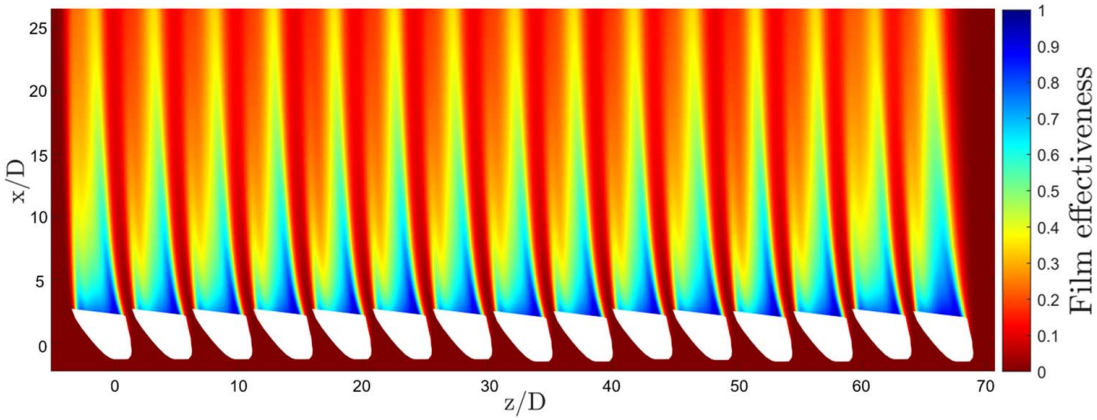

Fig. 15 CFD film effectiveness contour at BR = 1.2

mainstream. Although there are few, some RANS studies have been performed using the log-law modified for roughness such as the one by Lutum et al. [28] and Kang et al. [29] with good agreements found between experiments and CFD data, though only for parameters such as velocity profiles and Nusselt number (film effectiveness was not studied).

5 Results and Discussion

In this section, a comparison will be made between experimental results in the current study with studies available in the literature. Initially, the baseline geometry will be put into context with other baseline fan-hole studies on flat plate facilities. This comparison is intended to facilitate a comparison with the study of fan blockage by Whitfield et al. [4], also performed on a flat plate test facility. Experimental results will be compared with CFD results.

5.1 Performance of the Baseline Geometry. A contour plot of the baseline geometry for PR = 1.27 is shown in Fig. 14 with 15 film holes in the span. $x/D = 0$ was placed at the intersection of the film hole axis (cylindrical portion) and the blade surface. Three regions on the baseline blade were averaged in the span, and they are shown with colored boxes drawn on the figure and labeled "Tipwards," "Midspan," and "Hubwards." As aforementioned, three geometries were put on each test blade, with five film holes for each geometry. These regions represent the three middle film holes for the three film hole sets on each test blade. Geometries presented later will be compared to the performance of the baseline geometry in the same spanwise location of the blade. Figure 15 shows the result at the same conditions with CFD. It can be immediately seen that film effectiveness is overpredicted by CFD. It appears as if mixing between coolant and mainstream is underpredicted as found by Jones et al. [27]. Additionally, it can be seen that CFD does not capture the lateral spreading of the films seen in experiments, which was also seen in the study by Yu et al. [30] for late pressure surface fan-shaped holes. The overprediction by RANS CFD results was found for all geometries. Jones et al. [27] showed that RANS was much better at modeling velocity flow fields, and thus, CFD will be mostly used to provide an understanding of the flow field of each geometry. Figure 16 shows a comparison of the spanwise-averaged film effectiveness of the film holes in the three regions. A slight discrepancy is found in the film hole and immediately after the film hole exit. However, the performance of the films is very consistent across the span with at most 1–2% variation after a streamwise distance of $x/D = 5$. This variation is consistent with the work in the literature such as the study by Aghasi et al. [31]. A similar 3D printing method was used with comparable roughness-to-diameter ratios of $\mathrm{Ra}/D = 0.005 - 0.009$ (Polyjet and SLA). This suggests that minor variations such as the ones seen here are to be expected and the trend is that the data can be compared across the span.

Figure 17 shows a comparison between the baseline geometry of the current study and those in the studies by Whitfield et al. [4] and Schroeder and Thole [2] at BR = 0.5–0.6. Both studies implemented the "7-7-7"-shaped hole described in the literature on a flat plate test section, without lateral inclination. Note that blades numbered 1–3 refer to those described in Table 2. It should be noted that the x-axis was changed for this plot only. Data from the other two studies start with $x/D = 0$ at the downstream end of the fan, whereas in this study, $x/D = 0$ is located at the intersection between film axis and blade surface. This was due to the lateral

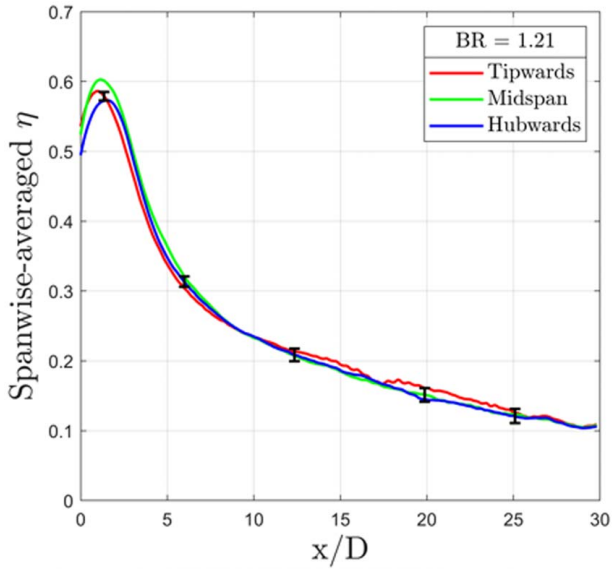

Fig. 16 Spanwise-averaged film effectiveness of considered regions

inclination resulting in no obvious datum from which to set the origin, such as in the other studies. A good agreement can be seen across test blades in the current study downstream of $x/D = 5$, while there is some higher variation near the exit of the fan. Discrepancies outside of uncertainty ranges might be attributed to minor geometric variations from the printing process, which might not be picked up by pin gauging of the film hole diameter. Additionally, the results of the current study align well with the baseline film holes tested by Whitfield et al. [4] and Schroeder and Thole [2].

One way to account for some of the geometric variation, such as pitch and film hole diameter, is to plot the results as area-averaged film effectiveness versus a scaled blowing ratio: mass flow per unit pitch, normalized by mainstream variables and hole diameter (from the study by Schroeder and Thole [2]). These data are shown in Fig. 18. Note that all studies compared with the current one were performed on a flat plate and averaged data over $x/D = 5 - 22$, except for the one by Yu et al. [30], which was performed on a pressure surface and averaged data over $x/D = 1 - 30$. Both averaged regions were given for the current study. Additionally, all studies

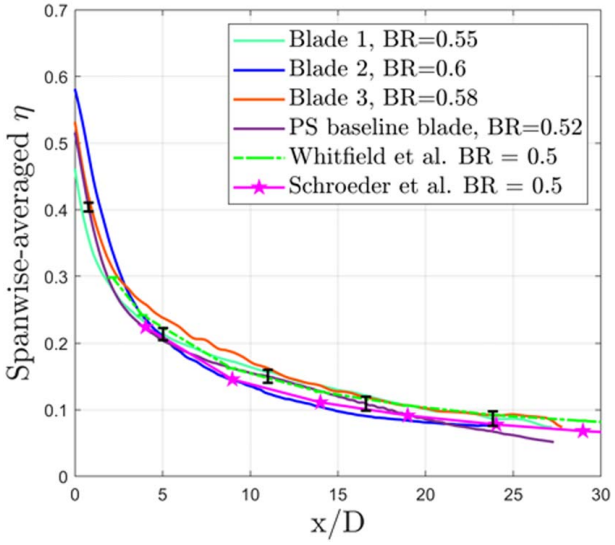

Fig. 17 Adiabatic film effectiveness for the baseline geometry at BR = 0.5

had straight holes, except for the current one. A comparison with flat plate studies shows that at low values of scaled blowing ratios, all perform very similarly. At higher values of scaled blowing ratios, the shaped hole of Heneka et al. [13] performed the worst, while the current study is close to the studies by Schroeder and Thole [2] and Whitfield et al. [4]. All of the geometries lift-off between scaled blowing ratio values between 0.15 and 0.2. Compared with Yu et al. [30], the current study only performs over a slightly smaller range of scaled BR, whereas that by Yu et al. [30] shows higher performance at low and high values of scaled BR.

Schroeder and Thole [2] showed that effective injection angle $\gamma = \alpha - \beta_{\text{fwd}}$ has a direct effect on film effectiveness with a lower γ leading to better cooling. This is explained in the study by Saumweber and Schulz [32]. The authors showed that both a lower expansion angle and a higher injection angle (and thereby also higher effective injection angle) led to more penetration of the coolant into the mainstream flow, which, in turn, leads to lower film effectiveness. The current study has an effective injection angle of 20.9 deg compared to 23 deg in the studies by Schroeder and Thole [2] and Whitfield et al. [4]. Heneka et al. [13] and Yu et al. [30] had higher effective injection angles of 25 deg and 35 deg, respectively (though Yu et al. [30] did not have a forward expansion). If the findings of lower γ, which leads to better cooling, were consistent between a flat plate and a concave surface such as the pressure surface here, the current study should outperform the flat plate studies. However, this is not the case, and it could be explained by the finding in the literature that suggests that a concave surface is usually detrimental to film effectiveness. Indeed, it has been shown that on concave surfaces, the presence of secondary flows known as Görtler vortices leads to an instability in the boundary layer and increases mixing [8]. This detrimental effect would counter an increase in film effectiveness that a shallower effective injection angle might bring about. It should, however, be noted that this might not be the only reason and the change in geometric features mentioned earlier and the addition of lateral inclination in the current study will have an effect on performance as well. The comparison with the study by Yu et al. [30] could shed some light on the effect of lateral inclination in the presence of curvature (despite some geometric variations in film holes that do not make it a perfect comparison). While both studies are similar for scaled BR between 0.13 and 0.24, the current study performs slightly worse at lower and higher scaled BR. This could support the finding in the literature that lateral inclination does not have much of an effect on film effectiveness.

5.2 Blockage Effects on Fan-Shaped Film Holes. Figure 19 shows adiabatic film effectiveness contours for all of the geometries at matched PR = 1.27 (most BR values are around 1.2 at this pressure ratio, with some outliers). The top row of contours represents geometries located at the tip of the blade, while the bottom row represents geometries located at midspan. Note that the baseline geometry has been included at both locations. The contours generally show good periodicity for the three film holes of each geometry. The film seems to slightly decay toward the most tipward-located hole (for instance, the green region of $\eta = 0.5$ ends at $x/D = 9$ for the leftmost hole and $x/D = 11$ for the rightmost hole of the baseline geometry). For the tipward geometries, the 0.4D globule slightly decreases film effectiveness near the film hole exit, and the high effectiveness region does not extend as far downstream. In contrast, the 50% lidded case creates a narrower film with high centerline values extending further downstream than the baseline case. The narrower film can be explained by a reduction in the film hole exit width (see Fig. 9). The fan exit deposition case performs quite similarly to the baseline case. Figure 20 shows N_2 mass fraction contours including velocity vectors for six geometries from CFD results. The 0.4D globule case does not seem to affect the flow field. If anything, the coolant layer looks slightly flatter than the baseline case, suggesting better attachment (this is also visible in Fig. 22, shown later). However, better attachment is not clear

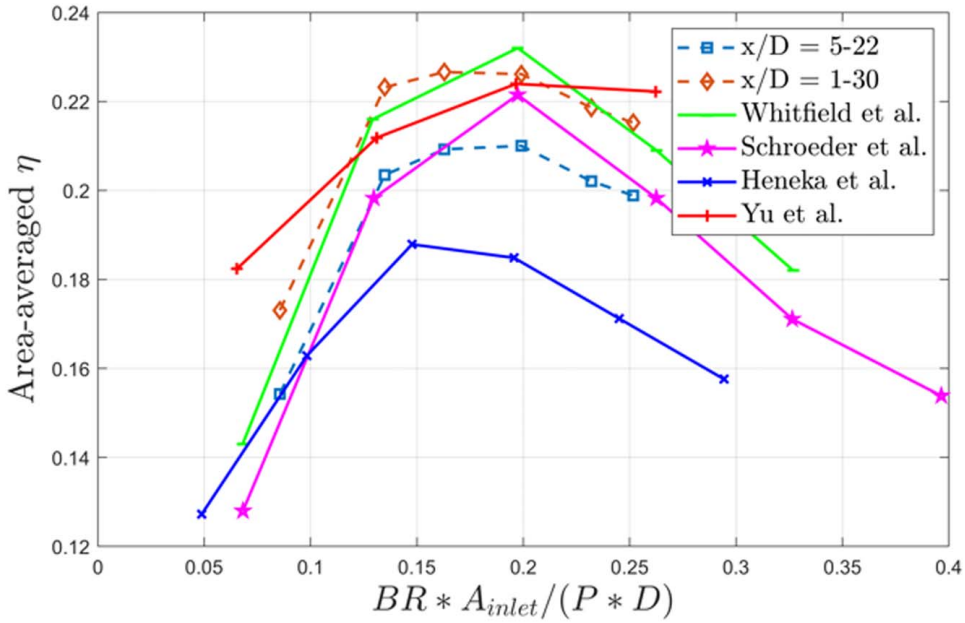

Fig. 18 Area average film effectiveness as a function of coolant flowrate per pitch

from the experimental finding in Fig. 19. Similarly, the fan exit deposition does not affect the flow field much. One might expect the hemispherical depositions to increase turbulence, but this does not seem to be the case. The 50% lidded case ejects the coolant slightly further into the mainstream than the baseline, resulting in a thicker coolant layer. In theory, this would deteriorate film effectiveness, but this does not seem to be the case from the experimental results.

For midspan geometries, a drop in film effectiveness can be seen for the 0.75D throat case compared to the baseline. The coverage is both narrower and does not extend as far downstream. This is most likely due to a lower mass flowrate at the same pressure ratio. Notice that this is the only bimodal film structure, possibly due to the larger AR (see Table 2). This bimodal structure was also seen in the study by Saumweber and Thole [32] at high lateral expansion angles, suggesting a change in the separation process of the film. The velocity field from CFD in Fig. 20 shows an overall lower level of N_2 mass fraction in the hole and at the surface, supporting the experimental finding of a lower coolant capacity. Similar to the 50% lidded case at the tip, the 25% lidded case appears to create a narrower film, which extends further downstream than the baseline. The 75% lidded case, in contrast, has much worse coverage. The film hole exit is much smaller than for the baseline, and the film stops performing much after $x/D = 10$. Similar to the blocked cases in the study by Whitfield et al. [4], the coverage is narrower and centerline film effectiveness is lower despite no reduction in C_D. This would suggest that the coolant lifts off into the mainstream and does not attach to the surface nearly as well. A possible explanation for the performances of the lidded cases can be found in studies of trenched film holes, which present the film hole with an edge perpendicular to the blade surface. In the study by Zhang et al. [10], the trench in fan-shaped holes on the concave surface was found to increase coverage length, similar to the 25% and 50% lidded cases. It is possible that the height of the lid in the 75% lidded case is past a critical value, and therefore, film effectiveness is much worse.

The CFD flow field in Fig. 20 supports the aforementioned observations for both the 25% and 75% lidded cases. The 25% lid initially ejects the coolant slightly more into the mainstream than the baseline case, but recovers quite quickly and does not affect the N_2 mass fraction much at the surface. In contrast, the 75% lid appears much more detrimental with higher velocity vector angles to the surface. Additionally, N_2 mass fraction is much lower at the surface of the blade than the baseline and 25% lidded cases. The increased mixing between coolant and mainstream likely results in the shorter coverage seen in the film effectiveness contour in Fig. 19. Figure 21 shows a line integral convolution plot of the 75% lidded case. The plot shows a recirculation region downstream of the lid as well as a point of reattachment slightly downstream. These are slightly less visible from the velocity vectors in Fig. 20 for the 75% lid case and are not present for the baseline, for instance.

Figure 22 shows N_2 mass fractions in a cross-sectional plane normal to the surface at $x/D = 3$. The differences among the baseline, 0.4D globule, fan exit deposition, and 25% lid cases are very subtle, supporting the previous experimental findings in the study by Fig. 19, as well as the similarity in the velocity field immediately downstream of the film hole exit in Fig. 20. Greater differences can be seen for the 50% and 75% lidded cases, which have narrower coolant films that extend higher into the mainstream. This increases mixing with the mainstream and ultimately reduces coverage. The 0.75D throat case shows a reduced coolant flow in the exit plane, as previously seen due to the reduced mass flowrate.

5.3 Performance of Experimental Data Against RANS Computational Fluid Dynamics. Area-averaged film effectiveness versus blowing ratio for the geometries are shown in Fig. 23. The area was taken from $5 \leq x/D \leq 22$, to reflect the range chosen in the literature and allow for a comparison. Note that the downstream edge of the film holes is located at $x/D = 2$. Results are split into tipward and midspan geometries, to allow for comparison with numerical results (experimental results are in bold lines and numerical results are in dashed lines). Both the 25% and 50% lidded cases perform slightly better than the baseline between $BR = 0.8 - 1.2$ and the 50% lid even appears to be better than the 25% lid in that same range (peaking at 0.23 and 0.22 area-averaged film effectiveness, respectively). The fan exit deposition is very similar to the baseline (within uncertainty ranges). The 0.75D throat lifts off at $BR = 0.8$, earlier than other cases without throat blockage. Additionally, it does not reach the same blowing ratios, which can be explained by the choice of inlet area and not the minimum throat area in the blowing ratio calculation (similar to other studies). The true blowing ratio would cover a higher range, close to that covered by the baseline geometry. It should also be noted that the choice of inlet area gives the 0.75D throat case a larger AR than other

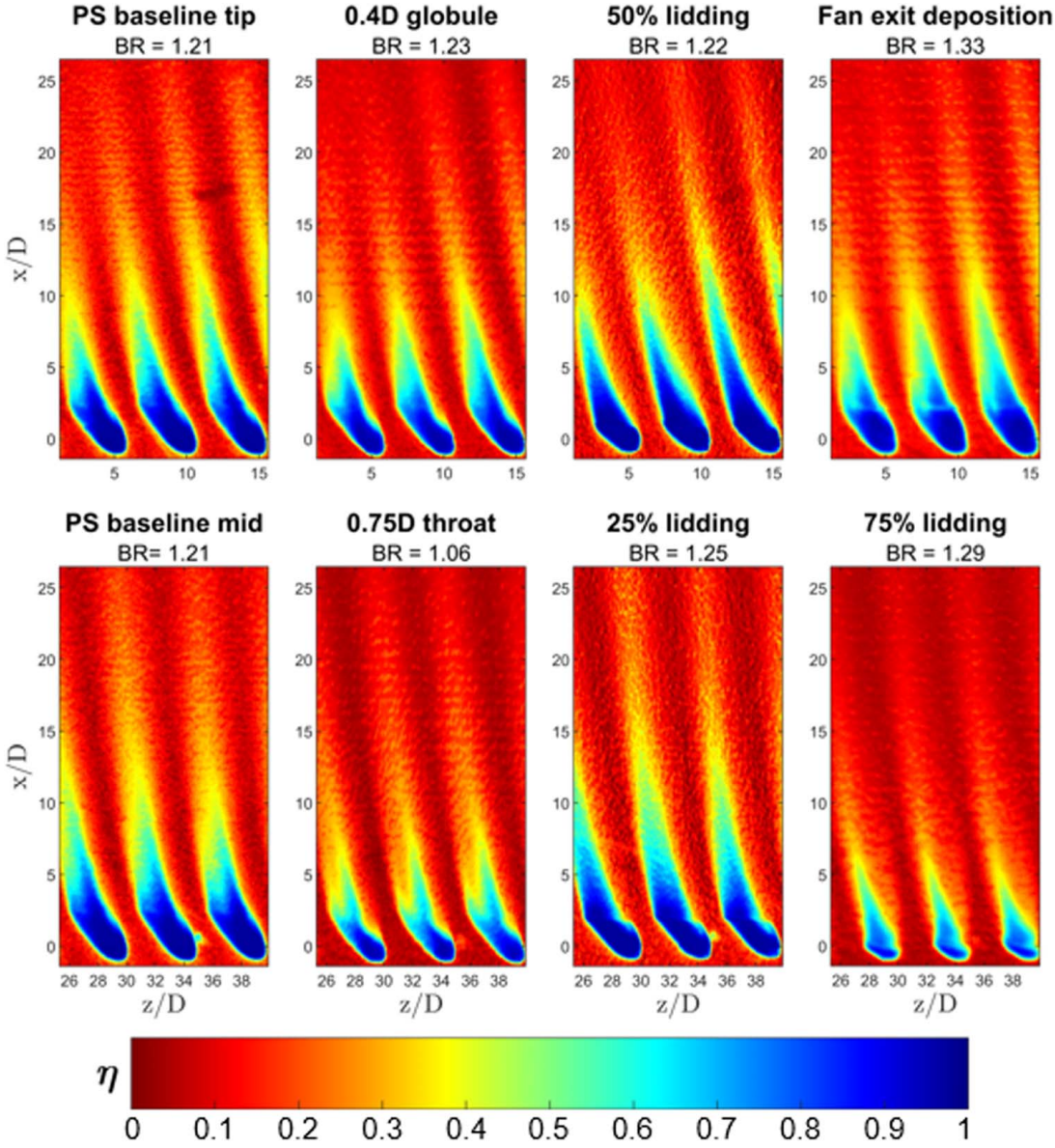

Fig. 19 Adiabatic film effectiveness contour for PR = 1.27 and DR = 1

geometries. In the literature, a larger AR generally delays coolant lift-off and improves film effectiveness for fan-shaped holes [33]. However, the opposite was found when the contraction in the 0.75D throat leads to a larger AR. It is possible that the 0.75D throat influences the separation process, and AR is past the point of optimal performance of the geometry. The 75% lidded case covers the same blowing ratio range as the baseline but has the worst cooling performance—almost half of the baseline. The 0.4D globule lifts off slightly earlier than the baseline (BR of 0.95 versus 1.1, respectively) though, given the close AR, the difference is not as large as for the 0.75D throat case. Overall area-averaged effectiveness is 0.04–0.05 worse overall than the baseline. The lidded cases appear to blow off at a BR of unity, similar to the baseline (BR between 1.0 and 1.1). This suggests that the lidding in the fan does not have a big effect on coolant lift-off, while blockage in the throat does.

When comparing each individual geometry's experimental and numerical results, it can be seen that the RANS CFD results overpredict film effectiveness across the board. It is known that despite being a time-efficient tool, RANS struggles to accurately predict absolute film effectiveness levels, partly due to the complexity of film cooling flow being injected into a cross-flow. As previously shown in Fig. 15, mixing between mainstream and coolant is underpredicted, thus leading to much better-predicted levels of film effectiveness further downstream of the film holes. Additionally, it has been seen in the literature that turbulent lateral diffusion is underpredicted due to the isotropic nature of the turbulence model [34]. This leads to an overprediction of effectiveness as well as a slower decay, both displayed in Fig. 15. An additional element to RANS CFD accuracy is mesh sensitivity as shown in the study by Jiang et al. [35]. Such a refined mesh such as the one presented in that study was, however, unfortunately not reproducible within the constraints of this study.

Despite this discrepancy with experimental results, the numerical results mostly display similar trends to most experimental results, making them a valuable tool for turbine designers to quickly assess the likelihood of the effect of a defect on film effectiveness compared to a pristine baseline film hole. Additionally, RANS models have previously been shown to be in strong agreement with experimental velocity fields [27]. For numerical results, the fan exit deposition and 25% lid had a close area-averaged effectiveness to the baseline; however, both reached maximum film effectiveness at BR = 1.4–1.5, compared to BR = 1.0–1.1 for experimental results. Both the 0.75D throat and 75% lid cases

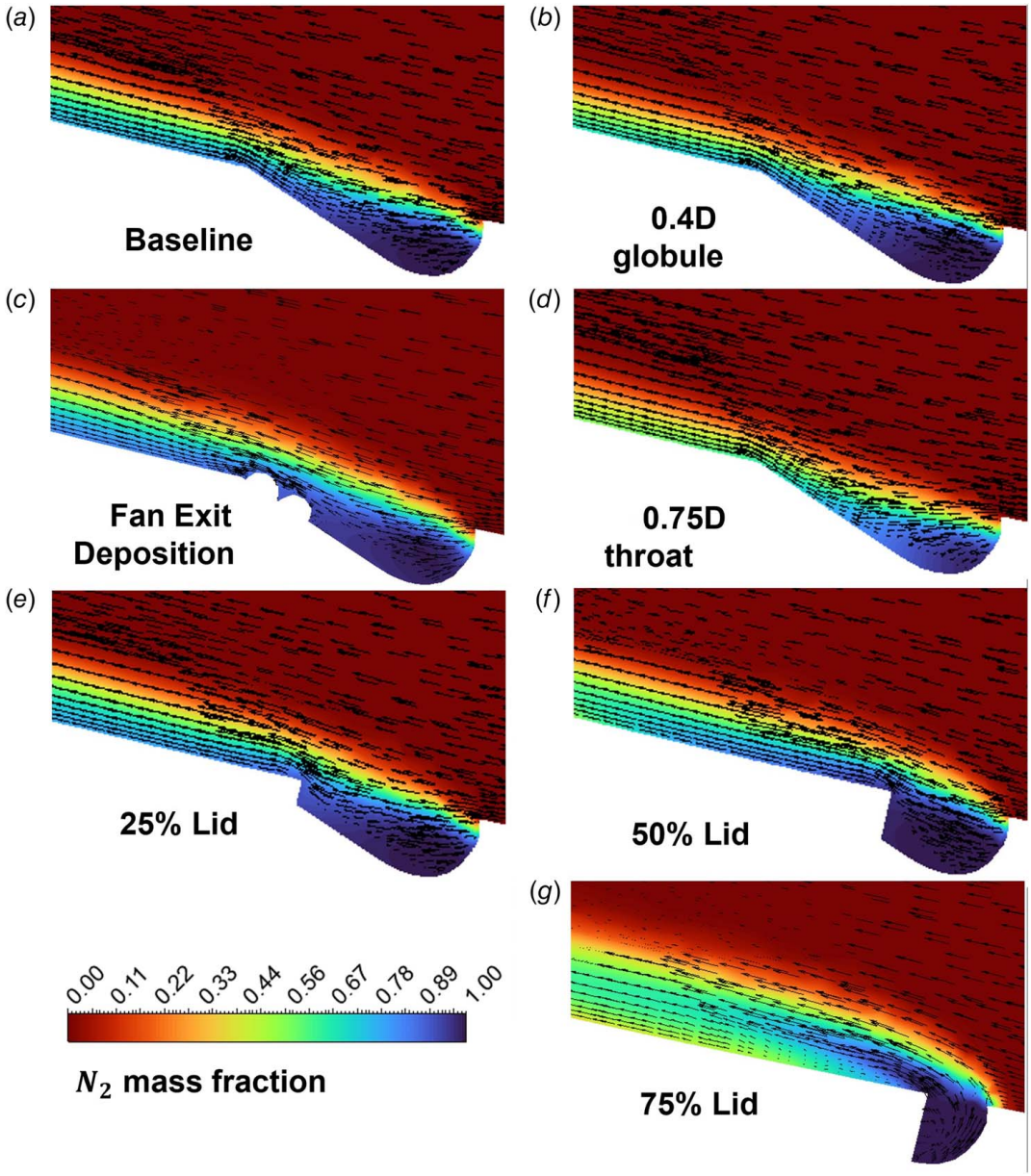

Fig. 20 CFD flow field of geometries in streamwise plane at PR = 1.27

predicted much lower levels than the baseline, peaking at BR = 0.9 and 0.7, respectively (compared to BR = 0.8 and 1 for experimental results). The 50% lid was predicted much worse than the baseline case, but much closer to experimental data. However, the curve for numerical results is much rounder and covers a larger range of BR than experimental data. The 0.4D globule case predicted a higher level, reaching a maximum effectiveness at BR = 1.7, compared to 0.95 for experimental data.

5.4 Effect of Geometries on Coolant Lateral Distribution. While spanwise and area-averaged plots give an understanding of the overall performance of a geometry, they do not capture the behavior of the films. This can be better understood when looking at lateral distribution of the coolant. Figure 24 shows lateral distributions averaged over three film holes, for tipward and midspan-located film holes at a streamwise distance of $x/D = 3$ (immediately after the film hole exit) and $x/D = 20$ (near the trailing edge). Note that $z/D = 0$ refers to the location of the origin in the most tipward-located film hole (not shown in Fig. 19). At $x/D = 3$, the baseline, fan exit deposition, and 0.4D cases have a similar behavior, showing a double peak in the coolant coverage with the higher peak being toward the hub of the test blade. However, the baseline has a higher centerline film effectiveness. The 50% lid looks slightly different in that the centerline of the film is pushed toward to tip of the blade. This can be explained by the design of the defect, which was built parallel to the film hole exit edge and thereby directs the coolant further to the tip. The same behavior can be observed for the 25% lidded case where the film is also shifted further toward the tip than the baseline film. The 0.75D throat has a double peak in the film, similar to the baseline, but the cooling performance is much worse on the whole. The 75% lidded case only shows one peak for the film and much worse peak effectiveness than the baseline. Additionally, the width of the film is much narrower than that of the baseline.

At $x/D = 20$, the baseline performance is much better than the other three geometries with a higher peak and trough effectiveness. While the 50% lidded case previously looked comparable to the baseline geometry in Fig. 23, the lateral distribution shows that

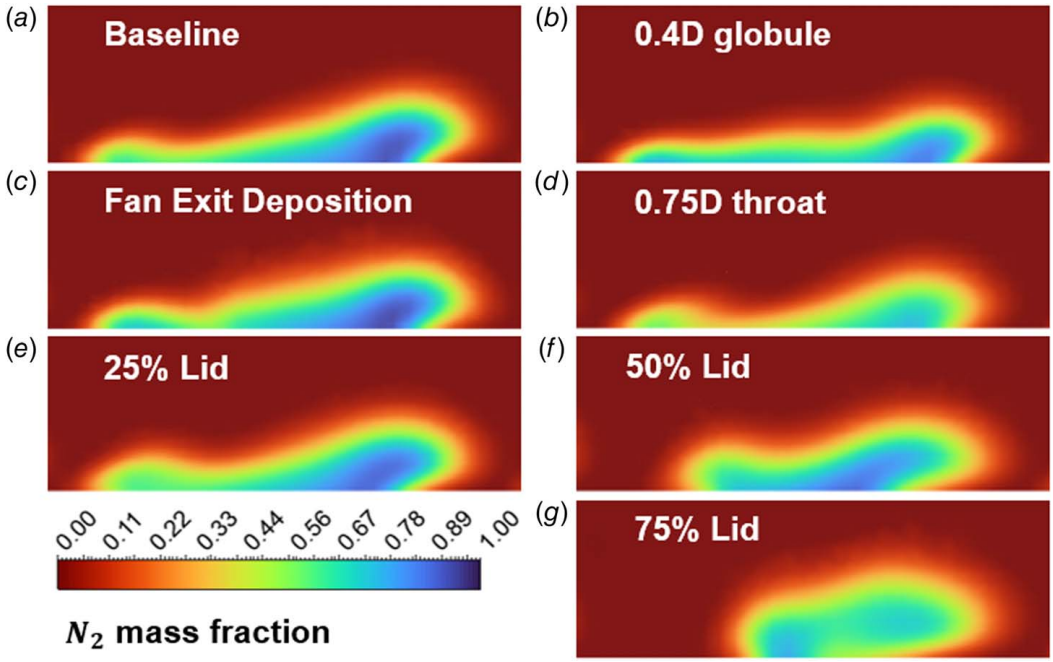

Fig. 22 CFD N_2 mass fraction contour plots of geometries in the cross-plane at $x/D = 3$ and PR = 1.27

this geometry has wider trough regions. In an engine, this region would likely have a higher metal temperature and therefore a higher risk of oxidation damage. The fan exit deposition and 0.4D globule cases have a similar behavior to the baseline but with lower overall performance and slightly worse trough regions. For tipward geometries at $x/D = 20$, the baseline performs the best with the highest peak and trough regions. The 25% lidded case shows a similar behavior to the baseline, though with a lower and wider trough region. Both the 0.75D throat and 75% lidded cases have even lower trough regions, which adds to their overall low performance in Fig. 23. It is acknowledged that the baseline cases appear different between the midspan and tipward plots at $x/D = 20$. While the films perform quite similarly when looking at a spanwise average plot such as shown in Fig. 16, the films of individual film holes do not perform in exactly the same way. Figure 14 shows that tipward-located geometries expand slightly toward the tip, while midspan film holes are slightly more in line with the mainstream direction. This is why geometries in Fig. 24 are only compared at the same location.

5.5 Performance of Lidded Geometries Relative to Literature. Figure 25 shows area-averaged film effectiveness versus scaled blowing ratio for lidded geometries. It can be seen that lidding in this study appears to be more lenient with effectiveness than in the study by Whitfield et al. [4]. A possible explanation for this is the difference in AR in the two studies. Lidding in the current study does not affect AR, which appears to dictate the point at which lift-off occurs. In the current study, lift-off for all the lidded geometries occurs at a scaled blowing ratio of 0.16. In contrast, the geometries in the studies by Whitfield et al. [4] lift-off earlier with increasing blockage, which correlates with a lower AR.

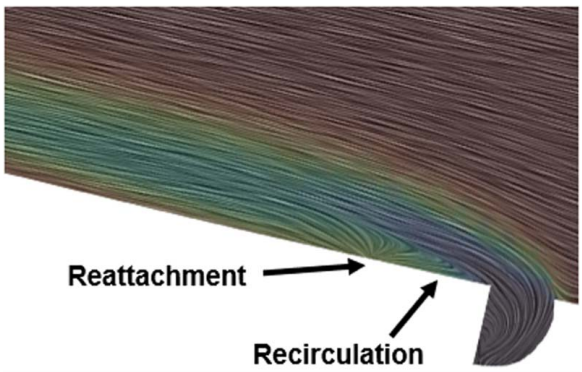

Fig. 21 Contour plot of 75% lid case with line integral convolution

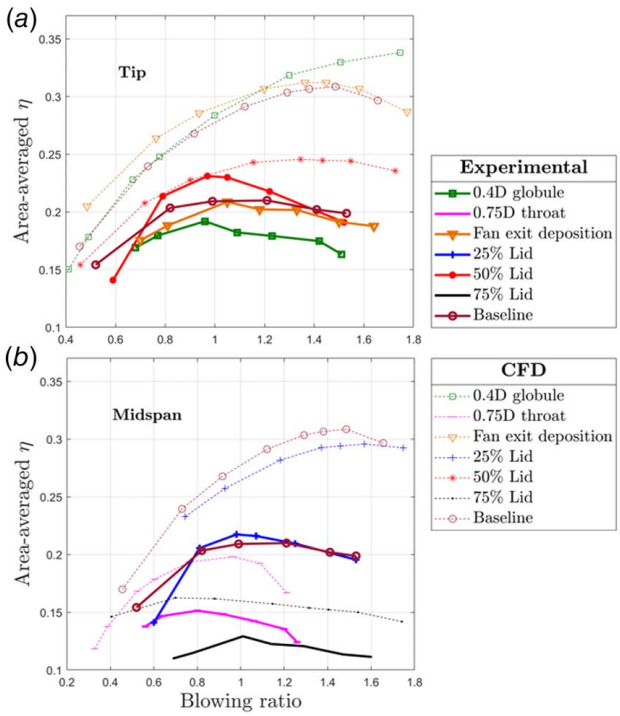

Fig. 23 Comparison between experimental and numerical area-averaged film effectiveness versus BR for geometries at the (*a*) tip and (*b*) midspan

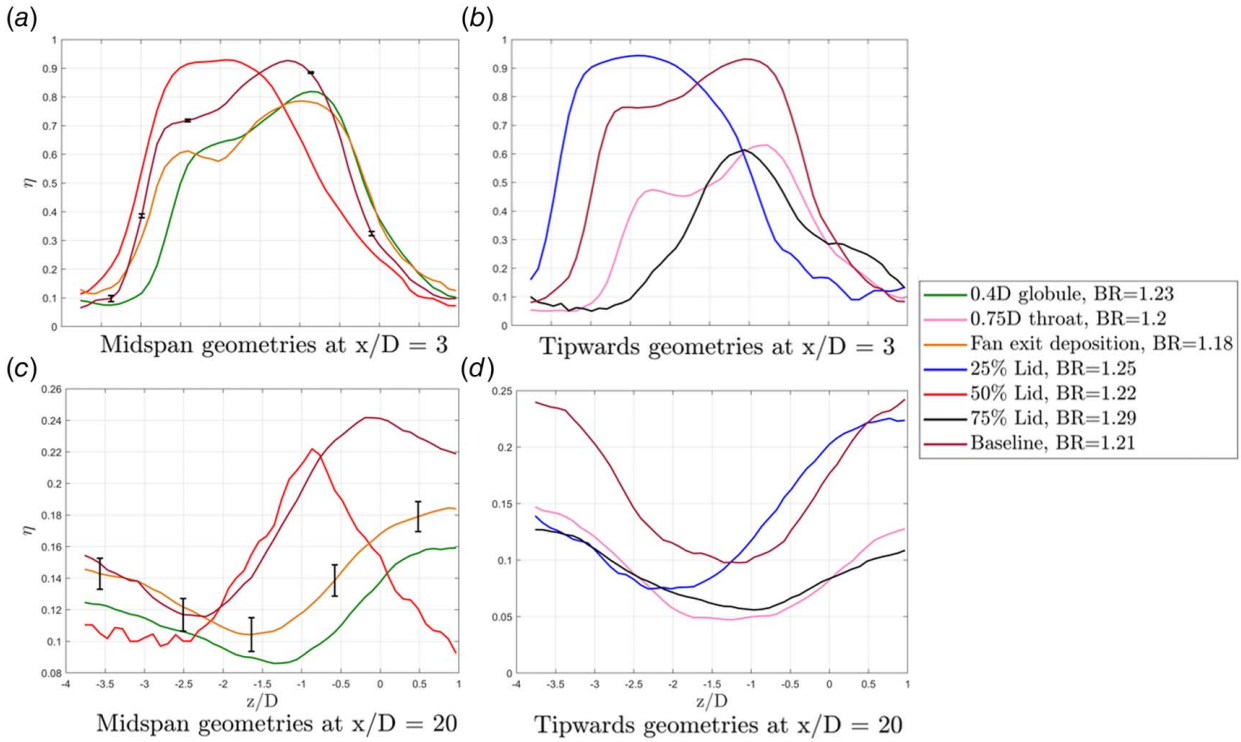

Fig. 24 Lateral distribution of film effectiveness between geometries at BR = 1.2 for (*a*) tipward and (*b*) midspan geometries at $x/D = 3$ and (*c*) tipward and (*d*) midspan geometries at $x/D = 20$

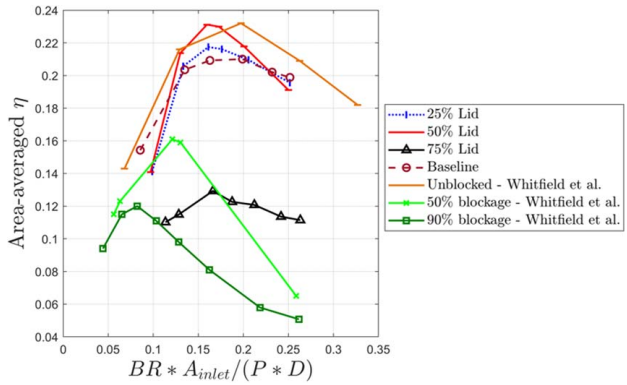

Fig. 25 Area-averaged film effectiveness versus coolant flowrate per pitch

6 Conclusion

The effects of blockages in fan-shaped holes on the pressure surface of a turbine blade were investigated. These results were compared with the results from steady RANS CFD in ANSYS FLUENT. The blockages studied corresponded to real imperfections found in film holes of engine-run and newly manufactured turbine blades.

Only blockages in the throat negatively affected C_D, through a reduction in mass flowrate. This correlated with lower levels of film effectiveness for the 0.75D throat and 0.4D globule cases than the baseline. Lidding created a narrower exit, leading to a narrower film, despite high centerline values. Additionally, all lidding cases showed lower trough effectiveness regions between individual films. Area-averaged film effectiveness for lidded cases was similar to the baseline up to a ratio of 50% lidding, while 75% lidding greatly deteriorated film effectiveness by ejecting coolant further into the mainstream. Fan exit deposition did not affect turbulence levels much in the film hole exit, which explains similar film effectiveness levels.

Peak area-averaged film effectiveness almost always occurred at a blowing ratio of around 1, except when blockages affected the throat of the film hole.

RANS CFD results were used to suggest explanations for the effect of blockages on film effectiveness. While absolute effectiveness levels were not accurately predicted, trends were observed, which still make RANS CFD a time-effective way to predict the performance of film cooling. More computationally expensive CFD simulations are required for an accurate prediction of film effectiveness levels on the turbine airfoil pressure surface.

Acknowledgment

The authors would like to thank the ongoing support provided by Rolls Royce PLC for this project. Additionally, the authors would like to thank Andreea Dabija, Liam Boland, Jason McCluskey, and Hal Surtell for the time invested in preparing test blades and experiments and in helping to improve the process along the way. We would like to acknowledge the use of the University of Oxford Advanced Research Computing (ARC) facility in carrying out this work.

Conflict of Interest

There are no conflicts of interest.

Data Availability Statement

The datasets generated and supporting the findings of this article are obtainable from the corresponding author upon reasonable request.

Nomenclature

l = contraction length of 0.75D defect
t = lid length in film hole plane
u = flow velocity
x = streamwise distance downstream of film hole exit

y = vertical distance from the blade surface
z = spanwise distance measured from tipwards film hole exit
C = total length of film hole exit in film hole plane
E = empirical constant in log-law velocity profile
P = pitch
R = radius of curvature
AR = area ratio (A_{exit}/A_{min})
BR = blowing ratio
DR = density ratio
PR = pressure ratio
α = injection angle
β = expansion angle for fan-shaped outlet
γ = effective injection angle
η = adiabatic film effectiveness
θ = lateral injection angle
κ = Von Karman constant
ρ = fluid density

References

[1] Dunn, M. G., 2012, "Operation of Gas Turbine Engines in an Environment Contaminated With Volcanic Ash," ASME J. Turbomach., **134**(5), p. 051001.
[2] Schroeder, R. P., and Thole, K. A., 2022, "Adiabatic Effectiveness Measurements for a Baseline Shaped Film Cooling Hole," ASME J. Turbomach., **144**(12), p. 121003.
[3] Bunker, R. S., 2000, "Effect of Partial Coating Blockage on Film Cooling Effectiveness," ASME Turbo Expo 2000: Power for Land, Sea, and Air, Munich, Germany, May 8–11.
[4] Whitfield, C. A., Schroeder, R. P., Thole, K. A., and Lewis, S. D., 2015, "Blockage Effects From Simulated Thermal Barrier Coatings for Cylindrical and Shaped Cooling Holes," ASME J. Turbomach., **137**(9), p. 091004.
[5] Jovanović, M., De Lange, H., and Van Steenhoven, A., 2008, "Effect of Hole Imperfection on Adiabatic Film Cooling Effectiveness," Int. J. Heat Fluid Flow, **29**(2), pp. 377–386.
[6] Wang, F.-q., Pu, J., Wang, J.-h., and Xia, W.-D., 2021, "Numerical Investigation of Effects of Blockage, Inclination Angle, and Hole-Size on Film Cooling Effectiveness at Concave Surface," ASME J. Turbomach., **143**(2), p. 021007.
[7] Zhang, J., Dong, W., Lin, J., Dai, H., and Wang, X., 2021, "Influence of Film Cooling Holes Partial Blockage on Cooling Effectiveness," ASME International Mechanical Engineering Congress and Exposition, Vol. 85673, American Society of Mechanical Engineers, p. V011T11A007.
[8] Schwarz, S. G., Goldstein, R. J., and Eckert, E. R. G., 1991, "The Influence of Curvature on Film Cooling Performance," ASME J. Turbomach., **113**(3), pp. 472–478.
[9] Bacci, T., Picchi, A., and Facchini, B., 2019, "Flat Plate and Turbine Vane Film-Cooling Performance With Laid-Back Fan-Shaped Holes," Int. J. Turbomach., Propul. Power, **4**(2), p. 14.
[10] Zhang, T., Pu, J., Zhou, W.-L., Wang, J.-H., Wu, W.-L., and Chen, Y., 2021, "Effect of Transverse Trench on Film Cooling Performances of Typical Fan-Shaped Film-Holes at Concave and Convex Walls," Int. J. Heat. Mass. Transfer., **175**, p. 121384.
[11] Ekkad, S. V., Zapata, D., and Han, J. C., 1997, "Film Effectiveness Over a Flat Surface With Air and CO_2 Injection Through Compound Angle Holes Using a Transient Liquid Crystal Image Method," ASME J. Turbomach., **119**(3), pp. 587–593.
[12] Gritsch, M., Colban, W., Schör, H., and Döbbeling, K., 2005, "Effect of Hole Geometry on the Thermal Performance of Fan-Shaped Film Cooling Holes," ASME J. Turbomach., **127**(4), pp. 718–725.
[13] Heneka, C., Schulz, A., Bauer, H.-J., Heselhaus, A., and Crawford, M. E., 2012, "Film Cooling Performance of Sharp Edged Diffuser Holes With Lateral Inclination," ASME J. Turbomach., **134**(4), p. 041015.
[14] Dittmar, J., Schulz, A., and Wittig, S., 2003, "Assessment of Various Film-Cooling Configurations Including Shaped and Compound Angle Holes Based on Large-Scale Experiments," ASME J. Turbomach., **125**(1), pp. 57–64.
[15] Ngetich, G. C., Ireland, P. T., and Romero, E., 2019, "Study of Film Cooling Effectiveness on a Double-Walled Effusion-Cooled Turbine Blade in a High-Speed Flow Using Pressure Sensitive Paint," ASME Turbo Expo 2019: Turbomachinery Technical Conference and Exposition, Phoenix, AZ, June 17–21.
[16] Han, J.-C., and Rallabandi, A., 2010, "Turbine Blade Film Cooling Using Psp Technique," Front. Heat Mass Transf. (FHMT), **1**(1), p. 013001.
[17] Miller, D. S., 1990, *Internal Flow Systems*, 2, revised edition, Vol. 5, BHRA (Information Services).
[18] Moffat, R. J., 1988, "Describing the Uncertainties in Experimental Results," Exp. Therm. Fluid. Sci., **1**(1), pp. 3–17.
[19] Wambersie, A., 2023, "High Porosity Cooling Features for Turbine Blade Applications," Ph.D. thesis, University of Oxford, Oxford, UK.
[20] Snyder, J. C., and Thole, K. A., 2020, "Performance of Public Film Cooling Geometries Produced Through Additive Manufacturing," ASME J. Turbomach., **142**(5), p. 051009.
[21] Gritsch, M., Schulz, A., and Wittig, S., 1998, "Discharge Coefficient Measurements of Film-Cooling Holes With Expanded Exits," ASME J. Turbomach., **120**(3), pp. 557–563.
[22] Schroeder, R. P., and Thole, K. A., 2017, "Effect of In-Hole Roughness on Film Cooling From a Shaped Hole," ASME J. Turbomach., **139**(3), p. 031004.
[23] Zamiri, A., You, S. J., and Chung, J. T., 2021, "Surface Roughness Effects on Film-Cooling Effectiveness in a Fan-Shaped Cooling Hole," Aerosp. Sci. Technol., **119**, p. 107082.
[24] Nikuradse, J., 1933, "Stromungsgesetze in Rauhen Rohren," vdi-forschungsheft, 361, p. 1. English Tanslation: Laws of Flow in Rough Pipes.
[25] Adams, T., Grant, C., and Watson, H., 2012, "A Simple Algorithm to Relate Measured Surface Roughness to Equivalent Sand-Grain Roughness," Int. J. Mech. Eng. Mechatron., **1**(2), pp. 66–71.
[26] Young, A., 1950, "The Drag Effects of Roughness at High Sub-critical Speeds," Aeronaut. J., **54**(476), pp. 534–540.
[27] Jones, F. B., Fox, D. W., and Bogard, D. G., 2019, "Evaluating the Usefulness of RANS in Film Cooling," ASME Turbo Expo 2019: Turbomachinery Technical Conference and Exposition, Phoenix, AZ, June 17–21.
[28] Lutum, E., Cottier, F., Crawford, M. E., Laveau, B., and Abhari, R. S., 2015, "A Computational Investigation of the Effect of Surface Roughness on Heat Transfer on the Stator Endwall of an Axial Turbine," Proc. Inst. Mech. Eng., Part A: J. Power and Energy, **229**(5), pp. 454–464.
[29] Kang, S.-H., Kang, Y.-S., and Han, K.-H., 2003, "Numerical Study on Blade Roughness Effect on the Performance of Turbomachines," Proceedings of the International Gas Turbine Congress, Tokyo, Japan, Nov. 2–7.
[30] Yu, Z., Li, C., An, B., Liu, J., and Xu, G., 2020, "Experimental Investigation of Film Cooling Effectiveness on a Gas Turbine Blade Pressure Surface With Diffusion Slot Holes," Appl. Therm. Eng., **168**, p. 114851.
[31] Aghasi, P., Gutmark, E., and Munday, D., 2017, "Dependence of Film Cooling Effectiveness on Three-Dimensional Printed Cooling Holes," ASME. J. Heat. Transfer-Trans. ASME., **139**(10), p. 102003.
[32] Saumweber, C., and Schulz, A., 2008, "Effect of Geometry Variations on the Cooling Performance of Fan-Shaped Cooling Holes," ASME J. Turbomach., **134**(6), p. 061008.
[33] Park, S. H., Kang, Y. J., Seo, H. J., Kwak, J. S., and Kang, Y. S., 2019, "Experimental Optimization of a Fan-Shaped Film Cooling Hole With 30 Degrees-Injection Angle and 6-Hole Length-to-Ddiameter Ratio," Int. J. Heat. Mass. Transfer., **144**, p. 118652.
[34] Kampe, T. a. d., Völker, S., Sämel, T., Heneka, C., Ladisch, H., Schulz, A., and Bauer, H.-J., 2013, "Experimental and Numerical Investigation of Flow Field and Downstream Surface Temperatures of Cylindrical and Diffuser Shaped Film Cooling Holes1," ASME J. Turbomach., **135**(1), p. 011026.
[35] Jiang, Y., Murray, A., di Mare, L., and Ireland, P., 2022, "Mesh Sensitivity of Rans Simulations on Film Cooling Flow," Int. J. Heat. Mass. Transfer., **182**, p. 121825.